crystals

MDPI

Review

Performance of $LiTaO_3$ Crystals and Thin Films and Their Application

Xuefeng Xiao [1,2,*], Shuaijie Liang [1,2], Jiashun Si [1,2], Qingyan Xu [1,2], Huan Zhang [1,2], Lingling Ma [1,2], Cui Yang [1,2] and Xuefeng Zhang [1,3]

[1] Key Laboratory of Physics and Photoelectric Information Functional Materials Sciences and Technology, North Minzu University, Wenchang Road 204, Yinchuan 750021, China
[2] College of Electric and Information Engineering, North Minzu University, Wenchang Road 204, Yinchuan 750021, China
[3] Ningxia Ju Jing Yuan Crystal Technology Company Limited, Shahu Road 304, Shizuishan 753000, China
* Correspondence: xuefengxiao@nmu.edu.cn

Abstract: Lithium tantalate ($LiTaO_3$, or LT) crystal is widely used in optical applications, infrared detection, and acoustic surface wave devices because of its excellent piezoelectric, pyroelectric, and nonlinear optical properties. In this paper, we discuss the defect structure of LT; the preparation method for LT; the influence of doping on LT; and LT's application in optical, acoustic, and electrical devices. We mainly analyzed the structure and physical properties of LT crystal, the preparation of LT crystal and LT thin films, the periodic polarization of LT crystal, the reduction of LT wafers, and the application potential of LT crystals in lasers and acoustic surface filters according to the most recent research. We also provide an overview of future research directions for LT in the fields of acoustics, optics, and other fields. The applications of LT in 5G, 6G, SAW filters, nonlinear optical devices, and waveguides are expected to provide additional breakthroughs.

Keywords: lithium tantalate; defect structure; performance control; application of lithium tantalate; piezoelectric crystal

Citation: Xiao, X.; Liang, S.; Si, J.; Xu, Q.; Zhang, H.; Ma, L.; Yang, C.; Zhang, X. Performance of $LiTaO_3$ Crystals and Thin Films and Their Application. *Crystals* **2023**, *13*, 1233. https://doi.org/10.3390/cryst13081233

Academic Editor: Yuui Yokota

Received: 26 May 2023
Revised: 6 July 2023
Accepted: 2 August 2023
Published: 10 August 2023

1. Introduction

Lithium tantalate ($LiTaO_3$, or LT) is widely used in filters [1], pyroelectric detectors, holographic memory devices [2], and other devices, due to its excellent piezoelectric, pyroelectric, and nonlinear optical properties. Some properties of LT are better than those of lithium niobate ($LiNbO_3$, or LN) [3], which is isomorphic to lithium tantalate. First, the photorefractive resistance of LT is twice that of LN [4]. Second, LT has a smaller temperature frequency coefficient (TCF) than LN, so it is an ideal material for manufacturing high-stability and broadband filters [5]. Finally, the thermal stability of LT, which is only 18 ppm in the range of 20–80 °C, is better than that of LN. Moreover, the optical damage threshold for LT at 514.5 nm is 1500 W/cm^2, which is approximately 37.5 times the optical damage threshold for LN, which is only 40 W/cm^2 [6]. Therefore, the performance of an LT device, after being fabricated into a specific device, is better than that of an LN device.

LT is also called a "universal crystal" because it has excellent electro-optic, nonlinear optical [7,8], piezoelectric, and pyroelectric properties. The applications of LT need to be perfected, and the preparation of large amounts of LT is still unable to avoid tantalate (Ta)-on-lithium (Li) site defects and Li vacancy defects [9]. This affects the applications of LT crystals in devices to varying degrees.

The pyroelectric coefficient of LT can be reduced by reducing and blackening LT wafers [10], which are periodically poled [11] and used for light-frequency converters. By doping other atoms to improve the relevant optical parameters [12], research into the properties of LT is able to provide a solid foundation for examining the infinite potential for the applications of LT.

The preparation methods for LT include the Czochralski method [13], the double-crucible Czochralski method [14], and the vapor-transport equilibrium method [15]. At present, the most popular method is the Czochralski method, which can grow large-size LT with many defects. Its defects mainly include Ta-on-Li site defects and Li vacancy defects [16]. These defects have some effects on the properties of LT, including changes to the Curie temperature [17], the coercive field [18], and photo-conductivity [19].

LT has been considered by scientists because of its excellent performance, its wide range of applications, and its adjustable usage. On the basis of these excellent features, in this paper, we discuss the structure of LT, the physical properties of LT, the defect types of LT, the growth methods of LT, the thin-film preparation of LT, the performance control of LT, and the applications of LT in optics and acoustics. Future research and applications of LT in acoustics and optics are proposed. It is expected that the applications of LT in 5G, 6G, SAW filters, nonlinear optical devices, and waveguides will achieve additional breakthroughs.

2. Crystal Structure and Physical Properties of Lithium Tantalate

Abrahams et al. [20,21] reported that LT belongs to the R3c space group at room temperature, as does LN, and the performance of LT is similar to that of LN. The structure of LT can be considered as the alumina-like corundum structure of Ta and Li ions along the c-axis [22]. The structure is shown in Figure 1.

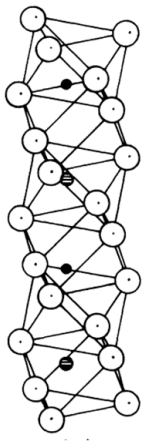

Figure 1. Structure of lithium tantalate: spatial structure of the unit cell. Open circles—O; solid circles—Li; cross-hatched symbols—Ta. Reprinted with permission from the authors of [23]. Copyright 1976, American Physical Society.

Table 1 shows that the melting point of LT crystal is 1650 °C [24], which is higher than that of LN. The Curie temperature of LT is lower than that of LN, and the pyroelectric coefficient of LT [13] is one order of magnitude higher than that of LN. Therefore, LT is more suitable than LN as a material for manufacturing pyroelectric detectors. Hang et al. [25] found that the elastic modulus of LT is 125 GPa, and the hardness of LT is about 10 GPa, while the elastic modulus of sapphire is 353 GPa, and the hardness of sapphire is 33 GPa. Thus, the hardness of LT is far less than that of sapphire. The material itself is brittle and prone to cracks during processing.

Table 1. Performance comparison between LT and LN [7,13,24–27].

Performance	Melting Point (°C)	Hardness (GPa)	Laser-Damage Threshold (W/cm^2)	Curie Temperature (°C)	Pyroelectric Coefficient (C/(m^2·K))
LT	1650	125	1500	610	2.3×10^{-4}
LN	1275		40	1210	4×10^{-5}

Miyazawa et al. [28] researched the binary phase diagram of LT and found that the congruent LT and the near-stoichiometric LT are different. The binary phase diagram is shown in Figure 2. It can be seen from the binary phase diagram that different compounds are produced with different raw material ratios. As a result of the decrease in Li content, the congruent LT has more defects than the near-stoichiometric LT. There are a sea of Li vacancies and Ta_{Li} defects. Therefore, the performance of congruent LT is worse than that of near-stoichiometric LT [29]. For example, it has a higher coercive field.

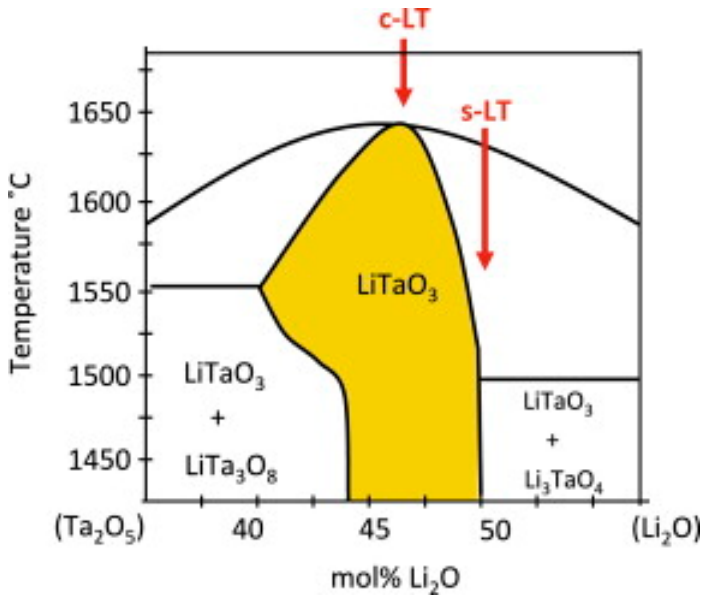

Figure 2. Binary phase diagram of LT. c-LT denotes LT concentric points, and s-LT denotes LT stoichiometric ratio points. Reprinted with permission from Ref. [30]. Copyright 2013, Elsevier.

3. Defect Types of $LiTaO_3$ Crystal

The defect structure of LT can be inferred by studying the defect structure of LN, which is isomorphic to LT. Lerner et al. [31] presented the most widely used model, namely the Nb anti-occupancy defect model, and this was extended by Kim et al. [32]. The Nb antisite defect is surrounded by three Li vacancies in the nearest neighborhood, and a fourth Li vacancy is located along the c-axis (referred to as the M1 model). In the defect model of LT, the Nb antisite defect is replaced by the Ta antisite defect, and the model is shown in M1 of Figure 3.

Due to the development of technology, Peterson [33] and Abrahams [34] proposed an alternative model to add a Nb vacancy to a Li site, based on ^{93}Nb NMR technology [32] and X-ray single-crystal diffraction data. Zotov [35] and Iyi [36] refined the model based on certain measurements, and in their model, all excess Nb in the octahedron was composed of Li vacancies. This model cannot explain the nonstoichiometric LT but can be used to study the defects of LT together with other defect models. Vyalikh [37] and others prepared two kinds of congruent LT using the Czochralski method. After heat treatment, the external diffusion of Li and the distribution of other defects were observed via electron spin resonance (ESR) spectroscopy, nuclear magnetic resonance (NMR) spectroscopy, and infrared (FT-IR) spectroscopy. It was found that the defects of LT prepared using the same method are quite different, so the same defect model cannot be used to represent the model of congruent LT.

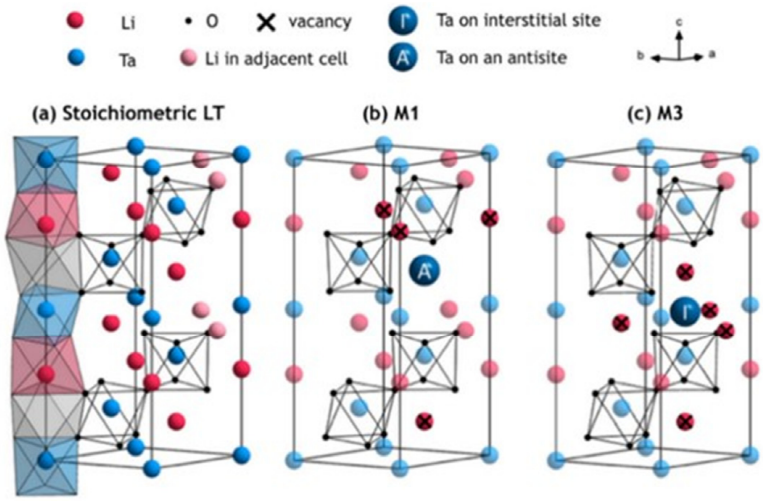

Figure 3. (**a**) Defect-free LT model; (**b**) defect model of LT with Li vacancy and Ta antisite defect; (**c**) defect model of octahedral LT with excess Ta in gaps and Li vacancy [37].

Based on the LN defect model's ESR (electron spin resonance), NMR (nuclear magnetic resonance), and FT-IR (infrared spectrum) results, Vyalikh et al. [37] proposed a more complex LT defect model, including central defects and external defects. The defect models include the Li vacancy model, the Ta antisite model, and some other mixed defect models. On the basis of the different Li content and growth conditions, the corresponding defect models are also different. Table 2 outlines the characteristics of a variety of defect models. In the M3 defect model, Ta enters the gap position and contains five Li vacancies, whose structure is shown in M3 in Table 2. In 2021, Masaif et al. [38] found that nonstoichiometric LT is more suitable to be described using the Li vacancy model combined with the Ta vacancy model, which is more consistent with its defect structure. In 2022, Xiao et al. [39] proposed a mixed defect model by analyzing Ta and Li valence changes in LT crystals with different Li contents, in which polaritons coexist with Li vacancies and Ta inversions. The new mixed defect model and the variation law of Ta valence with Li concentration proposed by this group provide a new direction and experimental basis for the study of the defects of near-stoichiometric ratio crystals, and the exploring of the Li content in LT under the best physical properties provides a theoretical basis.

Table 2. Defect clusters with different defect models, their concentrations, and defect formation energies in LT, Y_X^Z symbol, where the element Y is located at the position before X; Z denotes the relative charge (• is positive and ′ is negative); V and i denote vacancies and gaps, respectively; [a] indicates that the model may be present as a stabilizing defect in the congruent lithium tantalate along with other defective models [37].

Model	Central Defect	Compensating Defect	Reaction	Formation Energy (eV)
M1	$Ta_{Li}^{\bullet\bullet\bullet\bullet}$	$4V_{Li}^{\prime}$	$3Ta_2O_5 \rightarrow 5Ta_{Ta}^{x} + 15O_O^x + (1Ta_{Li}^{\bullet\bullet\bullet\bullet} + 4V_{Li}^{\prime})$	+1.94
M2	$5Ta_{Li}^{\bullet\bullet\bullet\bullet}$	$4V_{Ta}^{\prime\prime\prime\prime}$	$3Ta_2O_5 \rightarrow 1Ta_{Ta}^{x} + 15O_O^x + (5Ta_{Li}^{\bullet\bullet\bullet\bullet} + 4V_{Ta}^{\prime\prime\prime\prime})$	+10.90
M3	$Ta_i^{\bullet\bullet\bullet\bullet\bullet}$	$5V_{Li}^{\prime}$	$3Ta_2O_5 \rightarrow 5Ta_{Ta}^{x} + 15O_O^x + (1Ta_i^{\bullet\bullet\bullet\bullet\bullet} + 5V_{Li}^{\prime})$	+1.61
M3-1 [a]		$V_{Ta}^{\prime\prime\prime\prime\prime}$	$1LiTaO_3 \rightarrow 1Li_{Li}^{x} + 3O_O^x + (1Ta_i^{\bullet\bullet\bullet\bullet\bullet} + 6V_{Ta}^{\prime\prime\prime\prime\prime})$	+4.14
M4-1 [a]	$Ta_{Li}^{\bullet\bullet\bullet\bullet}$	$Li_{Ta}^{\prime\prime\prime\prime}$	$1LiTaO_3 \rightarrow 3O_O^x + (Ta_{Li}^{\bullet\bullet\bullet\bullet} + Li_{Ta}^{\prime\prime\prime\prime})$	+3.01
M5	$Ta_{Li}^{\bullet\bullet\bullet\bullet}, Ta_i^{\bullet\bullet\bullet\bullet\bullet}$	$9V_{Li}^{\prime}$	$6Ta_2O_5 \rightarrow 10Ta_{Ta}^{x} + 30O_O^x + (1Ta_{Li}^{\bullet\bullet\bullet\bullet\bullet} + 1Ta_i^{\bullet\bullet\bullet\bullet\bullet} + 9V_{Li}^{\prime})$	+7.16
M5-1		$4V_{Li}^{\prime}, V_{Ta}^{\prime\prime\prime\prime\prime}$	$3Ta_2O_5 \rightarrow 4Ta_{Ta}^{x} + 15O_O^x + (1Ta_{Li}^{\bullet\bullet\bullet\bullet\bullet} + 1Ta_i^{\bullet\bullet\bullet\bullet\bullet} + 4V_{Li}^{\prime} + 1V_{Ta}^{\prime\prime\prime\prime\prime})$	+1.94
M6	$Li_i^{\bullet}, Ta_i^{\bullet\bullet\bullet\bullet\bullet}$	$6V_{Li}^{\prime}$	$3Ta_2O_5 + LiTaO3 \rightarrow 6Ta_{Ta}^{x} + 18O_O^x + (1Li_{Li}^{\bullet} + 1Ta_i^{\bullet\bullet\bullet\bullet\bullet} + 6V_{Li}^{\prime})$	+7.03

In the reduction process of the LT crystal, there will also be an oxygen vacancy defect model. Kappers et al. [40] found that reduction will lead to the generation of oxygen vacancies, which contain two electrons, according to the analysis of the electron paramagnetic resonance (ESR) spectrum of the reduced wafer. By testing and analyzing black lithium tantalate chips, Wan et al. [41] found that black lithium tantalate chips have inherent oxygen vacancy defects. These defects increase the formation efficiency of Ta defects in the implantation process and further facilitate the preparation of lithium tantalate films using crystal ion slicing technology.

In conclusion, the defect structure of LT is complex. It mainly includes Li vacancies, Ta antisites, Ta vacancies, Ta entering the gap, and oxygen vacancy defects appearing on blackened wafers. LT with different Li contents is described by different defect models. The defect model of nonstoichiometric LT tends to be described using a mixed vacancy model.

4. Preparation of Lithium Tantalate

4.1. Growth of $LiTaO_3$ Crystals

The basic principle of the Czochralski method is the self-nucleation of LT on iridium wire with molten metal. A single-crystal rod is then produced by pulling it to a small diameter [42]. In 1963, Albert et al. [13] prepared LT using the Czochralski method for the first time and found that the material was ferroelectric, and the Curie temperature of the material was 665 °C.

In 1979, Brandle et al. [43] studied the reason for the cracking of large-size LT developed using the Czochralski method and found that the material's cracking has nothing to do with the quality of seed crystals. The cracking of LT is related to the defect density, and the quality of the crystal generated using the *y*-axis is better. Finally, large-size LT with a diameter of 4 cm and weight of 1200–1700 g were developed.

In 1995, Song et al. [44] used the Czochralski method to grow LT of good quality. By adjusting the temperature gradient, growth rate, and rotation rate, LT could be fabricated without macrodefects.

In 2006, Du et al. [45] used an iridium crucible, an improved temperature control system, an accurate power control system, and a suitable weighing system to grow five-inch LT to meet the market demand for large-sized LT. In addition, some companies have fabricated six-inch LT, but so far, there is no documented report. Figure 4 illustrates the four-inch 36°-RY $LiTaO_3$ single crystals using the Czochralski method.

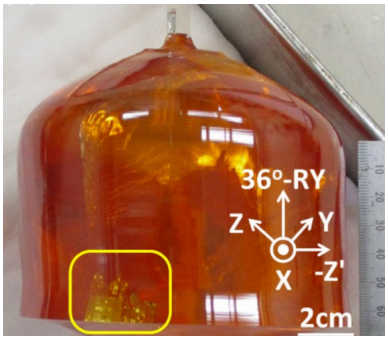

Figure 4. The 4-inch 36°-RY LiTaO3 single crystals using the Czochralski method [46].

Large-size $LiTaO_3$ crystals can be developed using the Czochralski method [45]. Due to the defects of this method, segregation occurs in the generated crystals. In addition, high thermal stress is introduced during crystal development using the Czochralski method, leading to dislocations that have little effect on properties [46]. From the point of view of optimizing the device performance, it is still necessary to improve and perfect the Czochralski method or find a new method for the preparation of large-size LT. In 2020, Yutaka et al. [46] studied the reason for the formation of twins in LT developed using the Czochralski method and found that the formation of twins was caused by the occurrence

of dislocations. The LT commonly used in commercial applications has a Li:Ta ratio of 48.5:51.5 in congruent lithium tantalate (CLT) [47]. The deficiency of lithium inside the CLT leads to many defects inside the crystal, so there are still many limitations in improving crystal performance and applications.

4.2. Preparation of Near-Stoichiometric Lithium Tantalate Crystals

Nearly stoichiometric lithium tantalate (NSLT) is a crystal with a Li:Ta ratio close to 1:1, with fewer defects and better properties. After recent advances, new methods have been proposed for the preparation of NSLT, including the K_2O cosolvent method [48–51], the horizontal-zone melting method [52] the double-crucible Czochralski method [53–55], and vapor transport equilibration (VTE) [15], all of which can be used to prepare lithium tantalate crystals with an internal Li content close to the stoichiometric ratio, but all of them also have different disadvantages. The K_2O cosolvent method and the horizontal-zone melting method require very precise control of the temperature field; the double-crucible Czochralski method allows for the production of NSLT crystals with better performance and a higher near-stoichiometric ratio, but it has not been widely promoted because of the complexity of the process, and only a few Japanese companies have fabricated NSLT using this method. In contrast, VTE is a simple method to produce NSLT crystals. In this approach, congruent wafers are simply heated in a crucible with a pre-reacted two-phase powder containing more lithium than a stoichiometric molar ratio. At high temperatures, there is a net transfer of lithium from the powder into the crystal through vapor transport and solid-state diffusion. In 2022, Xiao et al. [56] prepared NSLT via VTE and tested the electrical, thermal, and mechanical properties of NSLTs with different Li contents using the four-probe method and laser-pulse thermal conductivity tests. The maximum electrical conductivity measured was $4.4 \times 10^{-12}\ \Omega^{-1}\mathrm{cm}^{-1}$, and the maximum thermal conductivity reached 4.6 W/(mK). The development of NSLT fabrication technology provides more ways to enhance the quality of lithium tantalate crystals.

4.3. Preparation of $LiTaO_3$ Thin Films

Currently, the preparation methods for LT thin films mainly include the sol–gel method [57], the magnetron sputtering method [58], and the molecular beam epitaxy method [59]. In 1988, Imoto et al. [60] prepared $LiTaO_3$ thin films with the wet method, which can be used in humidity sensors. In 1993, Ye et al. [61] prepared LT thin films on monocrystalline silicon substrates using the sol–gel method. In 1995, Gitmans et al. [59] developed LT thin films with the oriented polycrystalline structure on a single-crystal silicon substrate via molecular beam epitaxy.

With the development of technology, the quality of $LiTaO_3$ thin films has improved in recent years. Sun et al. [62] used anhydrous acetic acid and tantalum ethanol as starting materials, propylene glycol as a solvent, and butyric acid to adjust the pH value, and thus prepared LT sol, which was heated to form LT films. The final test results revealed that annealing at different temperatures led to different optical band gaps. The advantage of the sol–gel method is that it can be cost-effective, but has the disadvantage of not being able to control the quality of the film. In 2019, Sun et al. [63] prepared $LiTaO_3$ thin films on various substrates via magnetron sputtering. With the increase in annealing temperature, the Li/Ta ratio changed, and the properties of the films improved. The films annealed at 700 °C for one hour were found to have the best properties, and they could effectively reduce Li and O vacancies. These films were relatively flat, and their grains were relatively uniform.

Yan et al. [64] prepared a $LiTaO_3$-on-insulator (LTOI) hybrid substrate with submicron lithium tantalate single-crystal films on silicon wafers through a direct bonding ion-cutting process. Using wafer bonding, the lithium tantalate crystal film was successfully bonded to the Si substrate, and the crystal quality was further improved via annealing at 400 °C. Wu et al. [65] prepared a fully insulating $LiTaO_3$-on-insulator (FI-LTOI) substrate and a trap-rich layer combined with a $LiTaO_3$-on-insulator (TR-LTOI) substrate by cutting the ion under the same conditions. Their research revealed that the quality factor of the resonator

prepared using the FI-LTOI substrate can be well maintained at 200 °C, and therefore it is an excellent substrate for 5G band SAW. Wan et al. [41] found that blackened lithium tantalate wafers have a higher foaming efficiency through their research on blackened lithium tantalate wafers, which is of great benefit for the preparation of lithium tantalate films using crystal ion slicing technology.

Ye et al. [66] prepared polycrystalline LT thin films using an improved molecular beam epitaxy (MBE) method. The ferroelectric properties of ultrathin $LiTaO_3$ films (<0.5 μm) developed on a silicon substrate were studied for the first time. The phase transition temperature was between 580 and 650 °C, the coercive field was 15–22 Kv/cm, and the surface spontaneous polarization was as high as 1 μC/cm^2. The pyroelectric current response was 100–200 μA/W. These experimental results show that $LiTaO_3$ is a promising material for infrared detector applications. Due to their excellent performance and cost-effectiveness, these films can be used in many applications, such as microdisk resonators [67], optical sensors [68], terahertz detectors [69], etc.

5. The Regulation of Properties of LT Crystals

5.1. Optical Properties of Doped LT

The photorefractive effect is a phenomenon in which the local refractive index is changed due to the spatial variation in light intensity. Holographic storage technology can produce holograms that can be stored and erased due to this effect [70]. The photorefractive properties of LT can be improved through doping with other elements. For example, LT doped with MgO periodically in poles has a high nonlinear coefficient (d_{33} = 13 pm/V) and a low threshold for optical damage [71–73].

In 2004, Imbrock et al. [74] studied the photorefractive properties of Fe-doped $LiTaO_3$ developed using the Czochralski method. They analyzed the dark storage time, which was determined using dark conductivity. In cases where the iron concentration is not too high, the dark conductivity mainly depends on the concentration of protons, as protons are mobile in the dark state. However, because of the small mobility of protons, they have a longer dark storage time. It can be seen from Figure 5 that the refractive index changes with the change in Fe ions' concentration, and this is independent of the wavelength of light. When the Fe-ion concentration reaches 300 × 10^{23} m^{-3}, the change in refractive index reaches its peak. At this time, the change in the refractive index of the crystal is the largest. The change in absorptivity at 310 nm is mainly related to Fe^{3+}, and the change in absorption at 400 nm is related to Fe^{2+}. By reducing the proton concentration through heat treatment, the dark storage time can be prolonged and is most sensitive to light at 400 nm. Thus, it can be used as a holographic storage material.

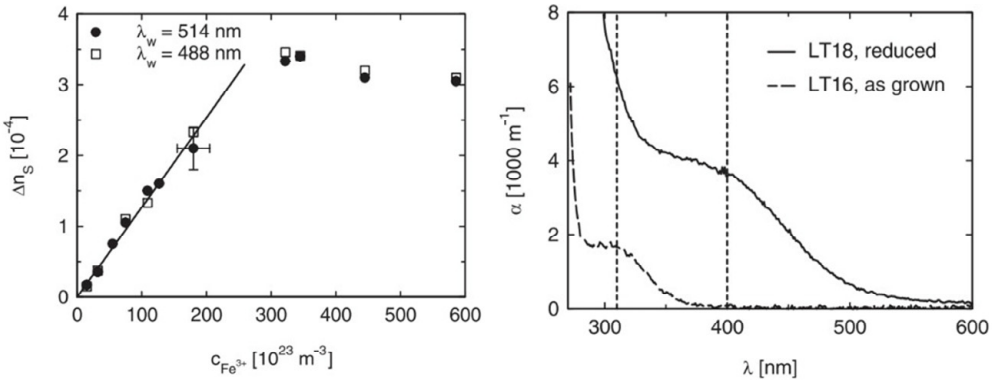

Figure 5. The figure on the left shows the change in refractive index Δn_s of Fe-doped LT with the concentration of Fe^{3+}. The figure on the right shows the change in the light absorption coefficient of LT with the increase in incident light wavelength. In the figure on the right, LT16 is LT doped with an Fe concentration of 10 × 10^{23} m^{-3}, and LT18 is LT doped with an Fe concentration of 190 × 10^{23} m^{-3}. Reprinted with permission from Ref. [74]. Copyright 2004, Springer Nature.

In 2015, Irzaman et al. [75] prepared La-doped $LiTaO_3$ thin films via magnetron sputtering. The addition of La promoted the formation of $LiTaO_5$ and reduced the energy gap. Doping with 10% La promoted the formation of hexagonal crystals. From the infrared spectrum, it was found that the higher the doping concentration, the greater the absorption of Ta-O and Li-O. Through the analysis with a particle size analyzer, it was found that the doping of lanthanum led to a decrease in particle size, whereas the refractive index of the $LiTaO_3$ film doped with 5% La increased, as shown in Figure 6. However, the refractive index of doped La was lower than that of undoped La.

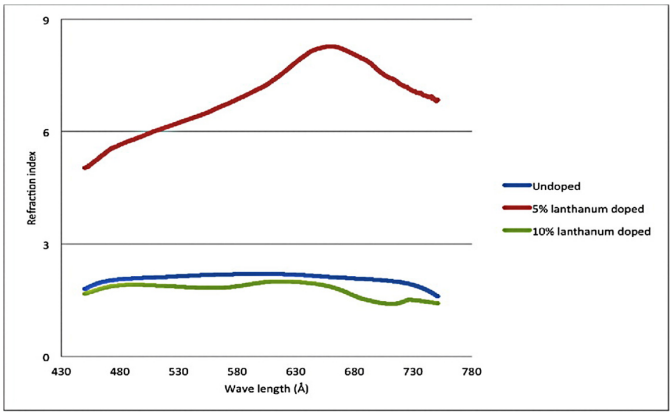

Figure 6. Effect of La doping with different concentrations on the refractive index of LT. Reprinted with permission from Ref. [75]. Copyright 2015, Taylor & Francis.

In 2018, Hao et al. [76] doped In and Nd in $LiTaO_3$ single crystals. This replaces the anti-Ta and Li vacancies, resulting in a reduction in the number of defects and an improvement in anti-light damageability. When the amount of In doping reached the threshold of 3%, the optical damage resistance threshold reached a maximum, and the photoelectric performance improved. In the same year, Yang et al. [77] found that doping Ga^{3+} in $LiTaO_3$ can improve the optical damage of waveguides, and the optical stability gain was 220 mW. It can be seen from Figure 7 that the maximum gain of the Ti:Er:LT waveguide measured at 220 mW of pump power is 1.0 dB/cm. By optimizing the process conditions and improving the overlap degree of Ga^{3+} and Er^{3+}, a higher optical gain can be obtained. These results highlight the potential of LT waveguides in photonic devices.

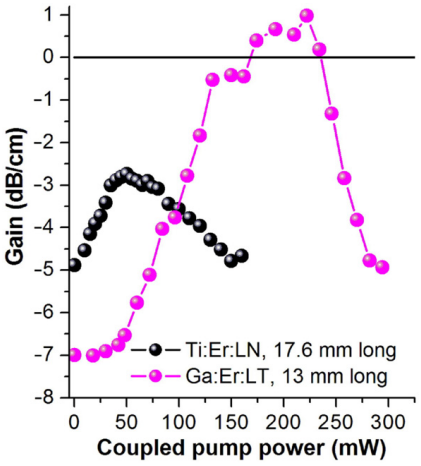

Figure 7. Optical gain of Ga:Er:LT waveguide (purple sphere) and Ti:Er:In waveguide (black sphere) as a function of the coupling 980 nm pump power. Reprinted with permission from Ref. [77]. Copyright 2018, Elsevier.

In 2020, Palatnikov et al. [78] doped Zn in $LiNbO_3$. Zn first occupied the position of Li ions, and then Zn occupied the position of Nb with increasing Zn. It was found that when the concentration of Zn reached 5% by mass, there was no photorefractive reaction under 160 W light irradiation, while the structure of the $LiTaO_3$ crystal was similar to that of $LiNbO_3$. It was also found that Zn-doped $LiTaO_3$ had a higher calcination temperature, as well as improved optical stability and uniformity; thus, it has the potential to be used as a new piezoelectric material.

It can be seen from Table 3 that $LiTaO_3$ doped with Fe can be used as a holographic storage material to record changes in lighting, which can improve the photorefractive performance of $LiTaO_3$. The doping of In, Ga, and Zn can improve the photorefractive ability of the materials. Doped La can be used as a laser material to change the refractive index and band gap of crystals.

Table 3. Effects of doping using various elements on the optical properties of $LiTaO_3$ crystals [74–78].

Doping Element	Performance Impact
Fe	The refractive index and absorption coefficient of $LiTaO_3$ crystals for different wavelength light intensities change, so they can be used as holographic storage material.
La	The refractive index of doped 5% lanthanum is higher, and the refractive index of doped 10% lanthanum is lower than that of undoped crystal.
In	It improves resistance to anti-light damage.
Ga	It improves resistance to anti-light damage.
Zn	The anti-photorefractive ability and optical stability are improved.

In conclusion, doping other elements can improve the properties of $LiTaO_3$, especially the refractive index, optical damage resistance threshold, optical stability, and optical uniformity. The doped LT can be used as holographic storage materials and new piezoelectric crystals; they are also expected to be used for lasers in future applications.

5.2. Reduction of $LiTaO_3$ Wafers

The results show that $LiTaO_3$ wafers have a high pyroelectric coefficient (2.3×10^{-4} C/(m^2·K)) and high transmittance. In the fabrication of SAW devices, a high pyroelectric effect will lead to charge accumulation and damage to the substrate pattern. In severe cases, the device may even be damaged, and high transmittance will also affect lithography, which is not conducive to wafer processing [79]. Therefore, previous researchers used the chemical reduction method to reduce the pyroelectric coefficient. After chemical reduction treatment, the wafer turned black, hence called a "lithium tantalate black wafer" [27,80].

The pyroelectric properties of $LiTaO_3$ are much better than $LiTaO_3$ blackened wafers. Xiao et al. [81,82] developed $LiTaO_3$ using the Czochralski method. After $LiTaO_3$ crystals were developed using the Czochralski method and crystal orientation for Y42° direction single circular wafer polishing, they were reduced with aluminum powder and silicon powder at 450 °C in a vacuum atmosphere for 40 h. Figure 8 shows the lithium tantalate flakes without reduction and reduced under different conditions, with obvious color change. Due to the evaporation of oxygen, the surface oxygen content of the reduced wafers significantly decreased. It was found that the reduction treatment could improve the conductivity of Lithium tantalate wafers, reduce the pyroelectric effect, and reduce the specific heat and Vickers hardness of lithium tantalate wafers, and had little effect on the Curie temperature. The high-temperature annealing of lithium tantalate before reduction treatment and other types of pre-treatment helped to reduce the stress inside the wafer, and it was easier to perform the blackening treatment to obtain a uniform blackened wafer. When the device was applied, it generated heat, leading to the surface charge accumulation of the device and thus performance degradation or breakdown of the device. Therefore,

reducing the pyroelectric properties improves the performance stability of some devices; for example, lithium tantalate black flakes are suitable for producing sound surface wave filters in comparison to lithium tantalate thin flakes.

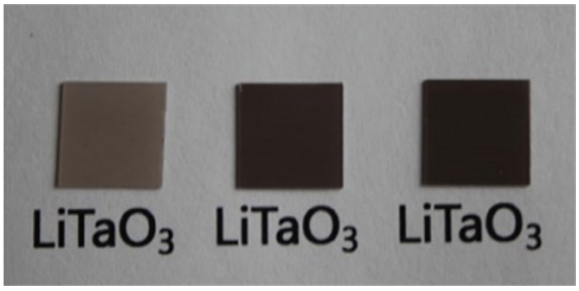

Figure 8. Unrestored $LiTaO_3$ sheet (**left**), reduced $LiTaO_3$ sheet (**right**, **middle**). Reprinted with permission from Ref. [81]. Copyright 2020, Springer Nature.

Yan et al. [79] used carbon powder and Li_2CO_3 powder to reduce the CLT sheet in nitrogen, and the thin, reduced $LiTaO_3$ sheet turned black without affecting the piezoelectric properties. Conductivity increased by 4–5 orders of magnitude, and resistivity changed to 10^9–10^{12} Ω·cm. Zhang et al. [83] used Zn powder and Si powder to reduce the LT wafer at 400 °C and found that the resistivity decreased significantly. It is believed that the reduction of Ta^{5+} to Ta^{4+} is the reason for the decrease in wafer resistivity.

Xia et al. [27] used H_2 and CO_2 to reduce $LiTaO_3$ wafers and found that this method can significantly reduce the pyroelectric coefficient. The obvious decrease in crystal transmittance is beneficial to wafer lithography. Zhang et al. [84] used LT black wafers to produce surface acoustic wave filters. When the ambient temperature changed from 25 °C to 100 °C, no electrostatic discharge waveforms exceeding 5 V were detected.

It can be seen from Table 4 that the resistivity of $LiTaO_3$ wafers was reduced using the chemical reduction method, so the pyroelectric effect was reduced. However, this slightly reduced the microhardness of the wafer but did not affect its piezoelectric effect.

Table 4. Parameters of $LiTaO_3$ wafers after blackening with different reducing agents [27,79,81,83].

Reducing Agent	Reduction Temperature	Color	Piezoelectric Constant d_{33} ($C \cdot N^{-1}$)	Resistivity (Ω·cm)	Shortcoming
Undoped		canary yellow	14×10^{-12}	4.25×10^{14}	
Al powder and Si powder	450 °C	grey		1.6×10^{11}	The specific heat and hardness slightly decrease.
C powder and Li_2CO_3 powder	460 °C	light gray	13×10^{-12}	5.1×10^{12}	Hardness slightly decreases.
C powder and Li_2CO_3 powder	540 °C	Black	13×10^{-12}	2.8×10^{10}	Hardness slightly decreases.
Zn powder and Si powder	400 °C	Brownish red	14.2×10^{-12}	2.83×10^{10}	

5.3. Periodic Polarization of $LiTaO_3$ Crystal

Periodic poling technology allows for the use of the maximal value of the nonlinear optical coefficient of $LiTaO_3$ and can be used for laser frequency doubling, frequency combining, frequency difference, optical parametric oscillation, and optical parametric amplification. Periodically poled lithium tantalate (PPLT) is one of the most transparent ferroelectric materials. It has high-frequency doubling efficiency in the ultraviolet band. At the same time, PPLT can be used as a second harmonic generation (SHG) [85].

Quasi-phase matching (QPM) in PPLT can be used for obtaining highly efficient frequency doubling. In 1962, Armstrong et al. [86] first proposed the quasi-phase matching technique. The quasi-phase matching technology can meet the phase matching of the second harmonic generation in $LiTaO_3$ to obtain high-frequency doubling conversion efficiency, which is not affected by the crystal orientation. Through periodic inversion, the frequency-doubling light is continuously superimposed to achieve a certain output power.

Because the birefringence of $LiTaO_3$ is not obvious, the phase velocity of fundamental frequency light and double-frequency light is not consistent, which limits the output of light. Therefore, QPM based on periodical poling is an important way to produce $LiTaO_3$ crystals for laser light frequency transformation [87].

PPLT doped with MgO by Surin et al. [88] is a kind of pump crystal with high efficiency for single-pass second harmonic generation. The nonlinear coefficient (d_{eff}) of the pump crystal is 9 pm/V, and the thermal conductivity (K) is 8.4 W/(m·°C). Figure 9 illustrates the periodically poled structure with a QPM period of 8 mm viewed under a phase contrast microscope after etching on the z surface.

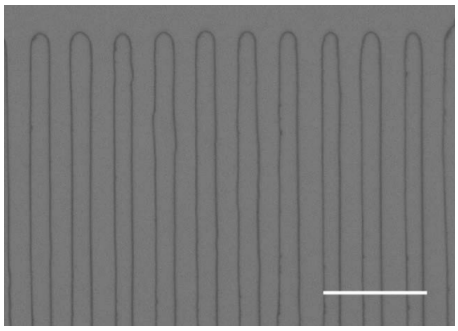

Figure 9. Periodically poled structure with a QPM period of 8 mm viewed under a phase contrast microscope after etching on the z surface. The marking is ~20 μm. Reprinted with permission from Ref. [54]. Copyright 2006, Elsevier.

In 2022, Zhang et al. [89] compared the nonlinear optical properties of lithium tantalate and lithium niobate crystals and determined that periodically polarized lithium tantalate crystals are more suitable for continuous laser frequency doubling from a technical research perspective. By designing and realizing a dual-optical multiplication with a periodic structure of 8.1 μm, a 540 nm continuous multiplication laser output of more than 5 W was obtained.

At present, PPLT has been applied to high-power green and blue lasers [90,91], optical parametric oscillators [92], etc. Although the technology is not fully developed, it can still be expected to be applied in the medical and military industries [93].

6. Application of $LiTaO_3$ Crystals

LT is one of the most widely used multifunctional optical crystals, which has many excellent properties such as electro-optic, nonlinear optical, ferroelectric, piezoelectric, pyroelectric, and acoustic properties [94]. These properties make $LiTaO_3$ suitable for use in a broad range of fields, such as integrated optics, pyroelectric detectors, optical waveguides, acoustic devices, etc. [95–99].

6.1. Integrated Optics

$LiTaO_3$ is a ferroelectric material, which has excellent electro-optic and nonlinear optical properties [100–103]. When rare-earth ions are doped in $LiTaO_3$, laser emission can be achieved, or it can be used as a laser pump source [104]. However, due to the broad effects of photorefractive properties in ferroelectric materials, the output power of the laser is limited [105], which is also the main reason why ferroelectric materials cannot be applied to lasers. To solve this problem, researchers found that doping MgO and rare-earth ions in $LiTaO_3$ can improve the photorefractive properties of the material and increase the threshold of photorefractive damage [106–109]. $LiTaO_3$ can be used to produce an ultrafast laser, which is an advantage that other lasers do not have [110]. In addition, $LiTaO_3$ can also be used in quantum communication and optical information processing in the optical field [111].

6.1.1. Laser Applications

Due to the good nonlinear optical properties and double-frequency and difference-frequency effects of $LiTaO_3$, these crystals have been widely used to make lasers and light modulators. In 2014, Feng et al. [112] studied Nd, Mg:$LiTaO_3$ lasers with a maximum pulse energy of 3.2 μJ. Due to the poor quality of Nd, Mg: $LiTaO_3$ crystals, the average output power is limited. In 2019, Chi et al. [110] used Ag implantation to embed Ag nanoparticles into $LiTaO_3$ and found that saturated Ag nano-ions embedded in $LiTaO_3$ would produce a unique local surface plasmon resonance (LSPR) effect. Based on this characteristic, a 1 μm Q-switched mode-locked laser based on a laser diode with a pulse width of 35 ps and a repetition rate of 8.74 GHz was developed. This shows that the $LiTaO_3$ laser has great potential in producing ultrafast lasers. LT has low loss in the visible light band and uniform birefringence [113], so it can be used to make light-intensity modulators. The principle of modulation is realized by using the linear electro-optic effect in single-domain $LiTaO_3$. LT is cut into rod shapes and coupled to the driving circuit as a lumped element. It was found that an optical extinction of about 15 dB could be achieved on a small-beam cross-section. However, the disadvantage of this type of modulator is that when the time for light to pass through the modulation crystal is close to the period of the modulation signal, the modulation efficiency begins to decline, and the light is difficult to focus.

It is not easy to produce lasers that directly generate visible light [114], so it has become a research hotspot for scientists to double the second harmonic generated by materials to develop a random Raman fire laser. In 2021, Cui et al. [114] developed a yellow laser that can convert an 1178 nm laser into a 589 nm laser with LT. The output power is 1.09 W, and the conversion efficiency is 10.8%. The experimental configuration is shown in Figure 10 below.

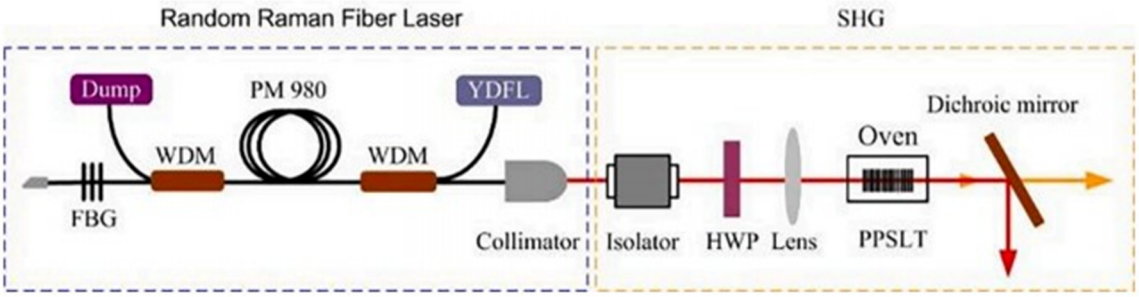

Figure 10. Experimental configuration diagram for generating the yellow laser light path. Reprinted with permission from Ref. [114]. Copyright 2021, Elsevier.

Although the technology for making laser or light intensity modulators with a $LiTaO_3$ crystal is not mature, at least we can see the application potential of the $LiTaO_3$ crystal in this field and the unique potential that other materials do not have.

6.1.2. Optical Communication and Optical Storage Applications

Ultraviolet transmission is a new means of information transmission. At present, technology is not very mature, but it has its unique advantages compared with conventional communication. First, UV light propagates in the form of scattering [92], so UV light can bypass obstacles. Second, it has strong anti-jamming ability and high confidentiality; Finally, UV communication can overcome the complex environment for communication. $LiTaO_3$ crystals have the potential to be used in UV communication [115].

Meyn et al. [116] polarized $LiTaO_3$ with an electric field of 23 KV/mm and finally measured the nonlinear coefficient as d_{eff} = 4.7 pm/V. In 2016, Rimeika [117] and others studied the femtosecond laser writing of Z-tangent $LiTaO_3$ and found that the n_o and n_e of $LiTaO_3$ can be changed, and a beam of light can be divided into two beams with orthogonal polarization, ordinary refractive index, and special refractive index. The waveguide with different refractive indices can be produced using different laser treatments of materials,

that is, the positive change in the refractive index (weak damage of multiple parallel damages), as well as gap and concave cladding (severe damage). It was found that the waveguide produced from $LiTaO_3$ can cause the intensity ratio of TE (the longitudinal component of the electric field is zero, and the longitudinal component of the magnetic field is not zero) and TM (the longitudinal component of the magnetic field is zero, and the longitudinal component of the electric field is not zero) of polarized light to be 1:1. This indicates that $LiTaO_3$ has the potential to perform all-optical information processing.

In 2020, Li et al. [118] studied the direct writing of Mg-doped periodically polarized near-stoichiometric lithium tantalate (PPMg-NSLT) using a femtosecond laser and found that ultraviolet light was generated in the cladding waveguide. Finally, the second harmonic generation (SHG) in the waveguide was successfully realized by using the quasi-phase-matching (QPM) method. It can be seen from Figure 11 that the wavelength of the generated secondary UV harmonic wave is 399.2 nm, and its insertion loss is less than 1.5 dB.

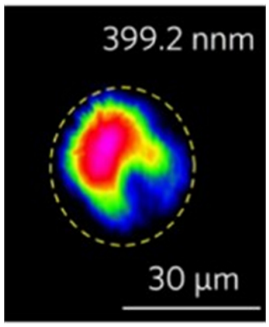

Figure 11. Near-field mode profiles of second harmonic 399.2 nm. Reprinted with permission from Ref. [119]. Copyright 2020, Elsevier.

In 2022, Wu et al. [120] reported an integrated 1×5 beam splitter based on an optical waveguide with Type I and Type II modifications for femtosecond laser writing in LT. The cladding waveguide composed of Type II modified tracks was used for optical signal transmission, photon crosstalk reduction, and the modulation of the mode field. While Type I single-line waveguides can be used to produce recoverable and rewritable beamsplitters, the rewritten structures still have good transmission performance; in addition, Type I modified waveguides can be rewritten quickly within 1–2 min. These beamsplitters show good performance in the output of programmable optical signals, which provides a possible strategy for developing erasable photonic data processors.

The quasi-phase-matching technique can cause $LiTaO_3$ to generate the second harmonic. The insertion loss is very small, and the nonlinear optical coefficient is relatively small. Therefore, periodically poled $LiTaO_3$ is suitable for application in the purple light range, so there is great hope it will be applied in purple light devices [116] in the future. PPLT doped with MgO may also be widely used in quantum communication in the future [118].

6.2. Applications of Pyroelectric Detectors

$LiTaO_3$ has the characteristics of a high pyroelectric coefficient, fast spectral response, and fast response speed. This material also has a high Curie temperature, good corrosion resistance, and other structural characteristics. Pyroelectric detectors are a type of detector based on the pyroelectric effect. Compared with conventional thermal infrared detectors, their advantage lies in their fast response speed. their principle is to respond to the change in the temperature change rate. Other heat detectors measure according to the temperature difference and need to reach a temperature balance quickly. In 2020, Dong et al. [119] researched on multifunctional terahertz detector, using a lithium tantalate sheet and a carbon nanotube absorption layer to form a sensitive terahertz pyroelectric detector device. The terahertz infrared detector was developed using some key technologies, and the final measured responsivity was 371.8 V/W.

The progress of devices depends on two aspects: the development of materials and the progress of processing technology. It has been found that the voltage response rate and the specific detectivity of the detector are directly proportional to the thickness of the pyroelectric infrared sensing unit [121]. Thinning and polishing are very helpful in improving the performance of infrared detectors. It has also been found that the pyroelectric coefficient is smaller when the crystal thickness is larger [122]. After that, the crystal surface is polished precisely to reduce the damage from the lattice of the surface so that the charge that enters the surface is released evenly, and the pyroelectric coefficient is also improved to a certain extent. Therefore, in order to improve the performance of the detector, we can improve the pyroelectric properties of materials or prepare thinner $LiTaO_3$ thin films.

Arose et al. [25] developed infrared detectors using LT and AlN. Compared with AlN, LT has a higher pyroelectric coefficient and a lower thermal absorption coefficient. The wavelength of the infrared detector fabricated from LT was found to be 5.6 μm. It had a higher specific detection rate than the AlN detector, and the light absorption rate reached 0.65. Because the thickness of $LiTaO_3$ was larger than that of AlN, the detection time was longer than that of AlN. This characteristic of LT thermal detectors will facilitate their use in specialized applications in the future.

6.3. Acoustic Applications

LT is famous for its low acoustic loss, high voltage electrical coupling coefficient, and excellent piezoelectric properties, which enables its wide application in the manufacture of SAW filters and resonators for mobile phones. At present, 70% of RF filters based on surface acoustic waves (SAWs) are manufactured from LT and LN single crystals. RF filters are generally used at frequencies below 2.5 GHz. In the 4G era, a mobile phone needs many filters. In the coming 5G era, mobile phones will need more SAW filters, and thus the performance of these filters deserves more attention.

A basic SAW filter consists of two interdigital transducers and a substrate with a piezoelectric effect in the middle [123]. The interdigital transducer (IDT) is a key device to convert electrical and acoustic signals. The main piezoelectric materials are quartz, LT, LN, and AlN [124,125]. The performance comparison of these materials is shown in Table 5. The electromechanical coupling coefficient of quartz is too small. The electromechanical coupling coefficient of LN is greater than that of LT, but its temperature coefficient is greater than that of LT. The performance of AlN is relatively good, so the three piezoelectric materials, LT, LN, and AlN, are widely used in the research of acoustic performance.

Table 5. Comparison of parameters of quartz and the three piezoelectric materials [6,44,116,125].

Piezoelectric Materials	TCF	Acoustic Surface Velocity	Electromechanical Coupling Coefficient	Temperature Coefficient
quartz		3158	0.14	0.2
AlN	−29 ppm	5130	6	
LN	−83 ppm	3895	0.62	52
Y165°LT	−18 ppm	3294	0.44	22

In 2010, Kim et al. [126] studied an interdigital transducer using LT as a substrate. Interdigital transducers have an active period (AP) and an inactive period (IP). When AP and IP are adjusted, the loss of the filter is reduced and the passband is narrowed, which indicates that the filter can have reduced loss and narrowed passband if its design is improved.

Due to the requirement of temperature stability, a crystal filter is generally more suitable for medium- and low-frequency filters, with tens of megabytes, and the core of the crystal filter is a resonator [127,128]. Crystal filters generate bulk acoustic waves (BAWs). Tanaka et al. [129] fabricated HAL SAW (hetero-acoustic-layer surface acoustic wave) resonators to measure frequency characteristics by using direct bonding between $LiTaO_3$ and the quartz substrate. The impedance ratio was 75 dB, the bandwidth was 5.1%,

and there were no obvious false responses below 14 GHz. In the same year, Ballandras et al. [130] fabricated a composite wafer from $LiTaO_3$ crystal and silicon, measured the TCF of the resonator, as shown in Figure 12, and found that the TCF was 18 ppm/K at 30–80 °C.

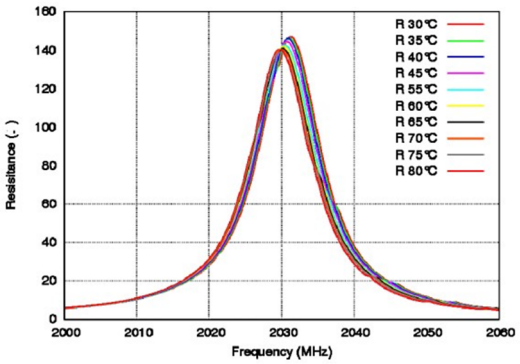

Figure 12. Frequency diagram of resistance at different temperatures. Reprinted with permission from Ref. [130]. Copyright 2015, Elsevier.

In 2019, Najoua et al. [131] fabricated high-frequency resonators using $LiTaO_3$ thin films. The resonant frequency was up to 5 GHz, the relative bandwidth was 7.3%, and the impedance ratio was 72 dB. It was found that the temperature frequency coefficient (TCF) was very small and therefore it could be applied to high-frequency resonators. The positive temperature frequency coefficient of quartz and the negative temperature coefficient of $LiTaO_3$ could be compensated. When optimal bonding was achieved, the TCF was only 2 ppm/°C. Therefore, crystal plane bonding technology is generally used to bond the two materials together to form resonators [129]. Naumenko et al. [132] bonded quartz and LT together to fabricate resonators with 75 dB impedance, 5.1% bandwidth, and no spurious response below 14 GHz. In 2020, Peng et al. [124] developed a crystal resonator, for which the center frequency was 63 MHz, the stopband loss was 76 dB, and the insertion loss was 4.6 dB.

In 2022, Hidetaka et al. [133] prepared an LTOI-based ring resonator and tested the device. It was found that the Q factor of the resonator reached 1.1 million. Wu et al. [65] tested an SH-SAW resonator on the FI-LTOI substrate, and its quality factor reached 4421. The TCF of the resonant and anti-resonant frequencies were 11.3 ppm/C and 9.1 ppm/C, respectively. The most important finding was that even at 200 °C, the Q value based on the FI-LTOI resonator remained good. SAW devices on the FI-LTOI substrate have great potential for low-loss and temperature-sensitive applications in RF wireless communication.

In conclusion, $LiTaO_3$-based RF filters and crystal resonators can be widely used in the future, and they are one of the important surface substrate materials for 5G communication in the future.

7. Expectations

$LiTaO_3$ has excellent piezoelectric, pyroelectric, and photorefractive properties, which make it possible to use in optical and acoustic fields. In recent years, research on the reduction of $LiTaO_3$ wafers and $LiTaO_3$ thin films has revealed that in some respects they have more suitable applications than $LiTaO_3$ due to having better properties. Although $LiTaO_3$ is a kind of crystal with excellent performance and has been applied in some fields, there are still some shortcomings in certain technologies.

First, the Czochralski method was optimized to prepare large-size, high-quality lithium tantalate crystals. Although the Czochralski method is still the main method for lithium tantalate growth, there are still many shortcomings in the development of LT, which limit the production of large-size high-quality LT. Improvements in the temperature field regulation and development process are important factors affecting the formation of LT, and the regulation of the temperature field system by improving the heating device and

the insulation layer of crystal formation is one of the important exploration directions for the development of large-size high-quality LT using the Czochralski method.

Secondly, there are new expectations to use LT films and NSLTs in future applications. LTs with the same composition are the most widely used LT, but lithium tantalate with the same composition itself has many defects, and these defects have led to the degradation of some properties of LT. In order to expand the range of LT applications, lithium tantalate thin films and NSLTs have become a new research hotspot. Lithium tantalate thin films have excellent applications in terahertz detectors, infrared material detectors, optical sensors, etc. NSLTs have fewer defects to help improve the performance of LTs and facilitate the future applications of LT.

Third, the optimization of the preparation of high-quality low-electrostatic black lithium tantalate wafers and refinement of the blackening mechanism. Because the most widely used LTs in commerce are still used in the application of sound surface filters, chemically reduced lithium tantalate wafers have smaller pyroelectric coefficients and therefore are more suitable for producing sound surface wave filters. Future filters will become smaller and smaller, but reduced lithium tantalate wafers are not easily developed into thin sheets due to their brittle mechanical properties. Thus, the thinning process during large-batch processing of wafers becomes more important. In addition, different preparation processes have a great impact on the quality and performance of blackened lithium tantalate wafers, but the study of the mechanism of lithium tantalate blackening is still unclear and will remain one of the key research directions in the future.

Finally, a new purposed area of application for lithium tantalate crystals is optical applications. The application of LT in optics is also one of the key concerns at present. Recent research revealed that LTs can be used to develop lasers, but this is still in the theoretical research stage, and the problem of the power output of lasers still restricts their application. Doping different ions in LTs can facilitate their use in different applications. The addition of active rare-earth ions can improve their application in laser matrix materials. The incorporation of a certain amount of anti-photodamage impurities can regulate the anti-photodamage characteristics of these crystals, thus expanding their application in electro-optical regulation and optical waveguides. The incorporation of photorefractive ions can enhance the photorefractive characteristics of LT crystals and improve their application in optical storage devices. Periodic polarization of lithium tantalate crystals can improve the nonlinear optical coefficient of LT, which grants it excellent advantages in frequency doubling, differential frequency, and optical parametric amplification applications based on quasi-phase-matching technology.

In short, because of their superior performance, $LiTaO_3$ crystals will have more applications in acoustic and optical fields in the future. Researchers also anticipate new breakthroughs in the investigation of $LiTaO_3$ crystals.

Author Contributions: All authors contributed to the study's conception and design. X.X. contributed to the organization of the final data and writing the first draft of the manuscript. S.L. mainly collected and organized data on the crystal structure and physical properties. Q.X. provided the summary of data on defect types. J.S. collected the content for the preparation of lithium tantalate. H.Z., L.M. and C.Y. collected the data on the properties of LT crystals. X.Z.'s main contribution was in the field of application, and all authors commented on previous versions of the manuscript. All authors have read and agreed to the published version of the manuscript.

Funding: This work is supported by the National Natural Science Foundation of China (61965001 11864001 and 61461001); the Fundamental Research Funds for the Central Universities; the North Minzu University (2020DXXY002 and 2021KJCX07); the Graduate Innovation Program of North Minzu University (YCX23122); the Ningxia Province Key Research and Development Program (2018BEE03015 and 2021BEE03005); the Ningxia Key Natural Science Foundation Project (2023AAC02045); the Natural Science Foundation of Ningxia (2019AAC03103 and 2020AAC03239); and the Ningxia First-Class Discipline and Scientific Research Projects (Electronic Science and Technology, No.NXYLXK2017A07-DKPD2023C10 and DKPD2023D01).

Data Availability Statement: The data pertaining to this report can be provided on a reasonable request.

Acknowledgments: The authors thank the Key Laboratory of North Minzu University (Physics and Photoelectric Information Functional Materials Sciences and Technology), the Ningxia Advanced Intelligent Perception Control Innovation Team, the Ningxia Acousto-optic Crystals Industrialization Innovation Team, and the Ningxia New Solid Electronic Materials and Devices Research and Development Innovation Team (2020CXTDLX12).

Conflicts of Interest: The authors declare no conflict of interest.

References

1. Gualtieri, J.G.; Kosinski, J.A.; Ballato, A. Piezoelectric materials for acoustic wave applications. *IEEE Trans. Ultrason. Ferroelectr. Freq. Control.* **1994**, *41*, 53–59. [CrossRef]
2. Hossain, A.; Rashid, M.H. Pyroelectric detectors and their applications. *IEEE Trans. Ind. Appl.* **1991**, *27*, 824–829. [CrossRef]
3. Katz, M.; Blau, P.; Shulga, B. Room temperature high power frequency conversion in periodically poled quasi-phase-matched crystals—Art. no. 687504. *J. Sci.-Adv. Mater. Dev. Vii* **2008**, *6875*, 87504.
4. Fang, S.; Ma, D.; Zhang, T.; Ling, F.; Wang, B. Growth and optical properties of Mg, Fe Co-doped $LiTaO_3$ crystal. *Optik* **2006**, *117*, 72–76. [CrossRef]
5. Fang, S.; Wang, B.; Zhang, T.; Ling, F.; Wang, R. Growth and photorefractive properties of Zn, Fe double-doped $LiTaO_3$ crystal. *Opt. Mater.* **2006**, *28*, 207–211. [CrossRef]
6. Mizuuchi, K.; Yamamoto, K. Characteristics of periodically domain-inverted $LiTaO_3$. *J. Appl. Phys.* **1992**, *72*, 5061–5069. [CrossRef]
7. Hatanaka, T.; Nakamura, K.; Taniuchi, T.; Ito, H.; Furukawa, Y.; Kitamura, K. Quasi-phase-matched optical parametric oscillation with periodically poled stoichiometric $LiTaO_3$. *Opt. Lett.* **2000**, *25*, 651–653. [CrossRef]
8. Imbrock, J.; Wevering, S.; Buse, K.; Krätzig, E. Nonvolatile holographic storage in photorefractive lithium tantalate crystals with laser pulses. *J. Opt. Soc. Am. B* **1999**, *16*, 1392–1397. [CrossRef]
9. Sánchez-Dena, O.; Villalobos-Mendoza, S.D.; Farías, R.; Fierro-Ruiz, C.D. Lithium niobate single crystals and powders reviewed—Part II. *Crystals* **2020**, *10*, 990. [CrossRef]
10. Yan, T.; Zheng, F.; Yu, Y.; Qin, S.; Liu, H.; Wang, J.; Yu, D. Formation mechanism of black $LiTaO_3$ single crystals through chemical reduction. *J. Appl. Crystallogr.* **2011**, *44*, 158–162. [CrossRef]
11. Lü, X.; Gang, Z.; Li, G.J.; Gao, Z.D.; Pan, S.D.; Zhu, S.N. Mid-infrared laser with 1.2 W output power based on PPLT. *Sci. China Phys. Mech.* **2010**, *5*, 638–642. [CrossRef]
12. Ma, D.C. *Growth, Structure and Properties of Zn Doped Lithium Niobate and Lithium Tantalate Crystals*; Harbin Institute of Technology: Harbin, China, 2007.
13. Albert, A.B. Growth of piezoelectric and ferroelectric materials by the CzochraIski technique. *J. Am. Ceram. Soc.* **1965**, *48*, 112–113.
14. Kim, I.G.; Takekawa, S.; Furukawa, Y.; Lee, M.; Kitamura, K. Growth of $Li_xTa_{1-x}O_3$ single crystals and their optical properties. *J. Cryst. Growth* **2001**, *229*, 243–247. [CrossRef]
15. Bordui, P.F.; Norwood, R.G.; Bird, C.D.; Carella, J.T. Stoichiometry issues in single-crystal lithium tantalate. *J. Appl. Phys.* **1995**, *78*, 4647–4650. [CrossRef]
16. Masaif, N.; Jebbari, S.; Bennani, F.; Hafid, M.; Jennane, A. Experimental and analytical study of defect structures in nonstoichiometric lithium tantalate and lithium niobate. *Phys. Status Solid B* **2003**, *240*, 640–648. [CrossRef]
17. Masaif, N.; Jebbari, S.; Bennani, F.; Jennane, A. New study of defect structure in nonstoichiometric lithium tantalate. *Ferroelectr. Lett.* **2005**, *32*, 7–22. [CrossRef]
18. Palatnikov, M.; Shcherbina, O.; Sandler, V.; Sidorov, N.; Bormanis, K. Effects of VTE treatment on composition of lithium tantalate single crystals. *Ferroelectrics* **2011**, *417*, 46–52. [CrossRef]
19. Jazbinšek, M.; Zgonik, M.; Takekawa, S.; Nakamura, M.; Kitamura, K.; Hatano, H. Reduced space-charge fields in near-stoichiometric $LiTaO_3$ for blue, violet, and near-ultraviolet light beams. *Appl. Phys. B* **2002**, *75*, 891–894.
20. Abrahams, S.; Hamilton, W.C.; Reddy, J. Ferroelectric lithium niobate. 4. Single crystal neutron diffraction study at 24 °C. *J. Phys. Chem. Solids* **1966**, *27*, 1013–1018. [CrossRef]
21. Abrahams, S.; Bernstein, J. Ferroelectric lithium tantalate—1. Single crystal X-ray diffraction study at 24 °C. *J. Phys. Chem. Solids* **1967**, *28*, 1685–1692. [CrossRef]
22. Marangoni, M.; Ramponi, R. Nonlinear Optical Waveguides in Stoichiometric Lithium Tantalate. In *Ferroelectric Crystals for Photonic Applications: Including Nanoscale Fabrication and Characterization Techniques*; Springer: Berlin, German, 2009; pp. 79–99.
23. Penna, A.; Chaves, A.; Andrade, P.d.R.; Porto, S.P. Light scattering by lithium tantalate at room temperature. *Phys. Rev. B* **1976**, *13*, 4907–4917. [CrossRef]
24. Ghambaryan, I.; Guo, R.; Hovsepyan, R.K.; Poghosyan, A.R.; Vardanyan, E.S.; Lazaryan, V. Creation of periodical antiparallel domain structure in lithium niobate crystals during growth process. *Ferroelectr. Lett. Sect.* **2003**, *30*, 59–67. [CrossRef]
25. Hang, W.; Zhou, L.; Shimizu, J.; Yuan, J.; Yamamoto, T. Study on the Mechanical Properties of Lithium Tantalate and the Influence on its Machinability. *Int. J. Autom. Technol.* **2013**, *7*, 644–653. [CrossRef]
26. Arizmendi, L. Photonic applications of lithium niobate crystals. *Phys. Status Solidi* **2004**, *201*, 253–283. [CrossRef]
27. Xia, Z.R.; Cun, K.; Xu, J.Y. Study on black lithium niobate and lithium tantalate crystals with weak pyroelectric effect. *J. Piezoelectrics Acoustooptics* **2004**, *26*, 126–128.

28. Miyazawa, S.; Iwasaki, H. Congruent melting composition of lithium metatantalate. *J. Cryst. Growth* **1971**, *10*, 276–278. [CrossRef]
29. Tian, L.; Gopalan, V.; Galambos, L. Domain reversal in stoichiometric $LiTaO_3$ prepared by vapor transport equilibration. *Appl. Phys. Lett.* **2004**, *85*, 4445–4447. [CrossRef]
30. Fujii, S.; Uda, S.; Maeda, K.; Nozawa, J.; Koizumi, H.; Fujiwara, K.; Kajigaya, T. Growth of congruent-melting lithium tantalate crystal with stoichiometric structure by MgO doping. *J. Cryst. Growth* **2013**, *383*, 63–66. [CrossRef]
31. Lerner, P.; Legras, C.; Dumas, J. Stoechiométrie des monocristaux de métaniobate de lithium. *J. Cryst. Growth* **1968**, *3*, 231–235. [CrossRef]
32. Kim, S.; Gopalan, V.; Kitamura, K.; Furukawa, Y. Domain reversal and nonstoichiometry in lithium tantalate. *J. Appl. Phys.* **2001**, *90*, 2949–2963. [CrossRef]
33. Peterson, G.E. ^{93}Nb NMR Linewidths in Nonstoichiometric Lithium Niobate. *J. Chem. Phys.* **1972**, *56*, 4848–4851. [CrossRef]
34. Abrahams, S.; Marsh, P. Defect structure dependence on composition in lithium niobate. *Acta Crystallogr. Sect. B Struct. Sci.* **1986**, *42*, 61–68. [CrossRef]
35. Zotov, N.; Boysen, H.; Frey, F.; Metzger, T.; Born, E. Cation substitution models of congruent $LiNbO_3$ investigated by X-ray and neutron powder diffraction. *J. Phys. Chem. Solids* **1994**, *55*, 145–152. [CrossRef]
36. Iyi, N.; Kitamura, K.; Izumi, F.; Yamamoto, J.; Hayashi, T.; Asano, H.; Kimura, S. Comparative study of defect structures in lithium niobate with different compositions. *J. Solid State Chem.* **1992**, *101*, 340–352. [CrossRef]
37. Vyalikh, A.; Zschornak, M.; Köhler, T.; Nentwich, M.; Weigel, T.; Hanzig, J.; Zaripov, R.; Vavilova, E.; Gemming, S.; Brendler, E. Analysis of the defect clusters in congruent lithium tantalate. *Phys. Rev. Mater.* **2018**, *2*, 013804. [CrossRef]
38. Masaif, N.; Lagrat, I.; Hboub, H. Curie temperature of nonstoichiometric lithium tantalate and lithium niobate by a mixed vacancy model. *Indian J. Phys.* **2021**, *96*, 411–417. [CrossRef]
39. Xiao, X.; Xu, Q.; Liang, S.; Zhang, H.; Ma, L.; Hai, L.; Zhang, X. Preparation and defect structure analysis of near-stoichiometric lithium tantalate wafers. *RSC Adv.* **2022**, *12*, 19091–19100. [CrossRef]
40. Kappers, L.; Sweeney, K.; Halliburton, L.; Liaw, J. Oxygen vacancies in lithium tantalate. *Phys. Rev. B* **1985**, *31*, 6792–6794. [CrossRef]
41. Wan, L.; Wu, C.; Yuan, Y.; Pan, X.; Shuai, Y.; Wu, C.; Zhu, J.; Zhang, W.; Luo, W. Enhanced surface blistering efficiency of H^+ implanted lithium tantalate by chemical reduction modification. *Appl. Surf. Sci.* **2023**, *622*, 156978. [CrossRef]
42. Bordui, P.F.; Norwood, R.G.; Bird, C.D.; Calvert, G.D. Compositional uniformity in growth and poling of large-diameter lithium niobate crystals. *J. Cryst. Growth* **1991**, *113*, 61–68. [CrossRef]
43. Brandle, C.D.; Miller, D.C. Czochralski growth of large diameter lithium tantalate crystals. *J. Infrared Technol.* **1979**, *3*, 53–58.
44. Song, L.; Li, M.H.; Xu, Y.H. Growth and physical properties of lithium tantalate crystals. *J. Synth. Cryst.* **1994**, *23*, 146–150.
45. Kang, P.; Zhang, Z.G.; Zhou, W.Q.; Wei, Y.; Zhang, H.P. Study on growth technology of 5-inch lithium tantalate crystal. *J. Synth. Cryst.* **1994**, *23*, 46–50.
46. Ohno, Y.; Kubouchi, Y.; Yoshida, H.; Kochiya, T.; Kajigaya, T. Twinning in Czochralski-Grown 36°-RY $LiTaO_3$ Single Crystals. *Crystals* **2020**, *10*, 1009. [CrossRef]
47. Xiao, X.; Si, J.; Liang, S.; Xu, Q.; Zhang, H.; Ma, L.; Yang, C.; Zhang, X. Preparation, Properties, and Applications of Near Stoichiometric Lithium Tantalate Crystals. *Crystals* **2023**, *13*, 1031. [CrossRef]
48. Zheng, W.; Wang, D.; Xu, Y. Growth and property of Zn-doped near-stoichiometric $LiTaO_3$ crystal. *J. Cryst. Growth* **2010**, *312*, 1879–1882. [CrossRef]
49. Baoshen, J.; Yequan, Z.; Xuefeng, Z. Research on defects and domain characteristics of MgO-doped near-stoichiometric lithium tantalate in room-temperature polarization process. *Sci. Bull.* **2010**, *5*, 11–15.
50. Zhang, X.F.; Lv, Z.W.; Jia, B.S. Flux Pulling Method of Growing Stoichiometric $LiTaO_3$ Crystal. *J. Synth. Cryst.* **2007**, *36*, 5.
51. Zhang, X.F.; Qiao, W.; Liu, J.; Jiang, T.S. Growth and characterization of near stoichiometric lithium tantalate crystals. *J. Rare Met. Lett.* **2007**, *09*, 23–26.
52. Shumov, D.P.; Rottenberg, J.; Samuelson, S. Growth of 3-inch diameter near-stoichiometric $LiTaO_3$ by conventional Czochralski technique. *J. Cryst. Growth* **2006**, *287*, 296–299. [CrossRef]
53. Kitamura, K.; Furukawa, Y.; Niwa, K.; Gopalan, V.; Mitchell, T.E. Crystal growth and low coercive field 180° domain switching characteristics of stoichiometric $LiTaO_3$. *Appl. Phys. Lett.* **1998**, *73*, 3073–3075. [CrossRef]
54. Kumaragurubaran, S.; Takekawa, S.; Nakamura, M.; Kitamura, K. Growth of 4-in diameter MgO-doped near-stoichiometric lithium tantalate single crystals and fabrication of periodically poled structures. *J. Cryst. Growth* **2006**, *292*, 332–336. [CrossRef]
55. Ganesamoorthy, S.; Nakamura, M.; Takekawa, S.; Kumaragurubaran, S.; Terabe, K.; Kitamura, K. A comparative study on the domain switching characteristics of near stoichiometric lithium niobate and lithium tantalate single crystals. *Mater. Sci. Eng. B* **2005**, *120*, 125–129. [CrossRef]
56. Xiao, X.; Xu, Q.; Liang, S.; Zhang, H.; Ma, L.; Hai, L.; Zhang, X. Preparation, electrical, thermal and mechanical properties of near-stoichiometric lithium tantalate wafers. *J. Mater. Sci. Mater. Electron.* **2022**, *33*, 20668–20677. [CrossRef]
57. Cheng, S.D.; Zhou, Y.; Kam, C.H. $LiTaO_3$ films with c-axis preferred orientation prepared on Si(111) substrate by sol–gel method. *Mater. Lett.* **2000**, *44*, 125–129. [CrossRef]
58. Combette, P.; Nougaret, L.; Giani, A.; Pascal-Delannoy, F. RF magnetron-sputtering deposition of pyroelectric lithium tantalate thin films on ruthenium dioxide. *J. Cryst. Growth* **2007**, *304*, 90–96. [CrossRef]

59. Gitmans, F.; Sitar, Z.; Günter, P. Growth of tantalum oxide and lithium tantalate thin films by molecular beam epitaxy. *Vacuum* **1995**, *46*, 939–942. [CrossRef]
60. Yamamoto, I.T. Preparation of lithium tantalate thin films by wet process and its application to a moisture-sensitive device. *Int. J. High Technol. Ceram.* **1988**, *95*, 520–525.
61. Ye, C.; Baude, P.; Polla, D.L. Characterisation of Ferroelectric Lithium Tantalate Thin Films Prepared by a Sol-Gel Process. *MRS Proc.* **1993**, *321*, 603. [CrossRef]
62. Sun, B.W.; Yang, M.; Gou, J.; Wang, J.; Jiang, Y.D. Preparation of $LiTaO_3$ thin films by sol gel method. *J. Univ. Electron. Sci. Technol.* **2020**, *49*, 283–286.
63. Sun, B.W.; Yang, M.; Gou, J.; Wang, J.; Jiang, Y.D. Preparation and crystallization properties of $LiTaO_3$ thin films by magnetron sputtering. *J. Semicond. Optoelectron.* **2019**, *206*, 55–58.
64. Yan, Y.; Huang, K.; Zhou, H.; Zhao, X.; Li, W.; Li, Z.; Yi, A.; Huang, H.; Lin, J.; Zhang, S. Wafer-scale fabrication of 42° rotated Y-cut $LiTaO_3$-on-insulator (LTOI) substrate for a SAW resonator. *ACS Appl. Electron. Mater.* **2019**, *1*, 1660–1666. [CrossRef]
65. Wu, J.; Zhang, S.; Chen, Y.; Zheng, P.; Zhang, L.; Yao, H.; Li, Z.; Zhao, X.; Huang, K.; Wu, T. Advanced Surface Acoustic Wave Resonators on $LiTaO_3/SiO_2$/Sapphire Substrate. *IEEE Electron Device Lett.* **2022**, *43*, 1748–1751. [CrossRef]
66. Tao, Y.; Gitmans, F.; Sitar, Z.; Pierhöfer, H.; Kündig, A.; Gamboni, I.; Günter, P. Dielectric, pyroelectric and structural properties of $LiTaO_3$ thin films grown on silicon by a modified molecular beam epitaxy. *Ferroelectrics* **1997**, *201*, 245–253. [CrossRef]
67. Xiongshuo, Y.; Liu, Y.A.; Ge, L.; Zhu, B.; Chen, X. High optical damage threshold on-chip lithium tantalate microdisk resonator. *Opt. Lett.* **2020**, *45*, 4100–4103.
68. Irzaman; Siskandar, R.; Nabilah, N.; Aminullah; Yuliarto, B.; Hamam, K.A.; Alatas, H. Application of lithium tantalate ($LiTaO_3$) films as light sensor to monitor the light status in the Arduino Uno based energy-saving automatic light prototype and passive infrared sensor. *Ferroelectrics* **2018**, *524*, 44–55. [CrossRef]
69. Wang, J.; Gou, J.; Li, W. Preparation of room temperature terahertz detector with lithium tantalate crystal and thin film. *AIP Adv.* **2014**, *4*, 97–105.
70. Jia, H. Nonvolatile luminescence storage properties of three doped stoichiometric lithium tantalate crystals. *J. Sci. Sin. Technol.* **2015**, *05*, 512–518. [CrossRef]
71. Zou, X.; Li, W.; Liang, H.; Liu, K.; Zhang, Y. 300 μJ, 3 W, few-cycle, 3 μm OPCPA based on periodically poled stoichiometric lithium tantalate crystals. *Opt. Lett.* **2019**, *44*, 2791–2794.
72. Kianirad, H.; Zukauskas, A.; Canalias, C.; Laurell, F. Domain dynamics in stoichiometric lithium tantalate revealed by wet etching and on-line second harmonic generation. *J. Appl. Phys.* **2017**, *121*, 184103. [CrossRef]
73. Hu, P.C.; Yin, J.G.; Zhao, C.C.; Gong, J.; He, X.M.; Zhang, L.H.; Liang, X.Y.; Hang, Y. Crystal growth, spectral and laser properties of Nd:LSAT single crystal. *Laser Phys.* **2011**, *21*, 1698–1703. [CrossRef]
74. Imbrock, J.; Baumer, C.; Hesse, H.; Kip, D.; Kratzig, E. Photorefractive properties of iron-doped lithium tantalate crystals. *Appl. Phys. B* **2004**, *78*, 615–622. [CrossRef]
75. Irzaman; Pebriyanto, Y.; Apipah, E.R.; Noor, I.; Alkadri, A. Characterization of Optical and Structural of Lanthanum Doped $LiTaO_3$ Thin Films. *Integr. Ferroelectr.* **2015**, *167*, 137–145. [CrossRef]
76. Hao, C.J.; Li, W.L.; Wang, J.M.; Gu, X.R.; Wu, T.; Liu, Y.W. Growth and optical properties of In and Nd doped lithium tantalate single crystal. *J. Acta Opt. Sin.* **2018**, *38*, 254–259.
77. Yang, X.-F.; Zhang, C.-Y.; Zhang, Z.-B.; Pun, E.Y.-B.; Zhang, D.-L. Low-loss Ga: Er: $LiTaO_3$ optical waveguide for integrated optics. *Mater. Lett.* **2018**, *227*, 199–201. [CrossRef]
78. Palatnikov, M.N.; Masloboeva, S.M.; Arutyunyan, L.G. Synthesis of Zinc-Doped Lithium Tantalate Charge in the Technology of Novel Crystalline Functional Materials. *Russ. J. Appl. Chem.* **2020**, *93*, 645–653. [CrossRef]
79. Shen, J.; Bobkowski, R. Black lithium niobate SAW device fabrication and performance evaluation. In Proceedings of the Ultrasonics Symposium, 2000 IEEE, San Juan, Puerto Rico, 22–25 October 2000.
80. Standifer, E.; Jundt, D.; Norwood, R.; Bordui, P. Chemically reduced lithium niobate single crystals: Processing, properties and improvements in SAW device fabrication and performance. In Proceedings of the 1998 IEEE International Frequency Control Symposium (Cat. No. 98CH36165), Pasadena, CA, USA, 27–29 May 1998; pp. 470–472.
81. Xiao, X.; Zhang, H.; Zhang, X. Preparation, electrical, thermal and mechanical properties of black lithium tantalate crystal wafers. *J. Mater. Sci. Mater. Electron.* **2020**, *31*, 16414–16419. [CrossRef]
82. Xiao, X.; Xu, Q.; Zhang, H.; Ma, L.; Hai, L.; Zhang, X. Preparation and surface morphology of black lithium tantalate wafers. *Optoelectron. Adv. Mater. -Rapid Commun.* **2022**, *16*, 364–372.
83. Zhang, X.F.; Liang, B.; Zhou, W.T. Preparation of low pyroelectric lithium tantalate crystals by reduction of Zn powder. *J. Rare Met. Lett.* **2011**, *30*, 58–60.
84. Zhang, X.H.; Cheng, Y.G.; Zhu, Y.; Chen, S.Q. Study on pyroelectric effect of acoustic meter filter. *J. Piezoelectrics Acoustooptics* **2017**, *39*, 797–799.
85. Mizuuchi, K.; Yamamoto, K. Generation of 340-nm light by frequency doubling of a laser diode in bulk periodically poled $LiTaO_3$. *Opt. Lett.* **1996**, *21*, 107–109. [CrossRef] [PubMed]
86. Armstrong, J.; Bloembergen, N.; Ducuing, J.; Pershan, P.S. Interactions between light waves in a nonlinear dielectric. *Phys. Rev.* **1962**, *127*, 1918–1939. [CrossRef]

87. Zhang, X.T. *Frequency Doubling Effect of Femtosecond Laser Direct Writing Periodically Polarized Lithium Tantalate Waveguide*; Shandong University: Jinan, China, 2019.
88. Surin, A.A.; Borisenko, T.E.; Larin, S.V. Generation of 14 W at 589 nm by frequency doubling of high-power CW linearly polarized Raman fiber laser radiation in MgO:sPPLT crystal. *Opt. Lett.* **2016**, *41*, 2644–2647. [CrossRef] [PubMed]
89. Zhang, L.F.; Xie, D.K.; Chen, H. Research on continuous laser frequency doubling technology based on periodically polarized lithium tantalate crystal. *J. Laser Infrared* **2022**, *52*, 6.
90. Jiao, M.L.; Lv, X.J.; Liu, C.; Yuan, H.; Qi, Y.F.; Ding, Y.Q.; Zhao, G.; Zhou, J. Characteristics of periodically polarized lithium tantalate frequency doubled narrow line all fiber CW laser amplifier. *J. Chin. J. Lasers* **2012**, *39*, 30–34.
91. Ma, Y.; Peng, X.C. Study on red and blue light generated by 1342 nm laser through periodically polarized lithium tantalate. *J. Chin. J. Lasers* **2005**, *02*, 262–264.
92. Wei, X.B.; Peng, Y.F.; Wang, W.M.; Chen, X.W.; Wang, J.H.; Xie, G. Research on optical parametric oscillator based on periodically polarized lithium tantalate crystal. *J. Acta Opt. Sin.* **2011**, *31*, 152–156.
93. Samanta, G.K.; Fayaz, G.R.; Ebrahimzadeh, M. 1.59 W, single-frequency, continuous-wave optical parametric oscillator based on MgO:sPPLT. *Opt. Lett.* **2007**, *32*, 2623–2625. [CrossRef]
94. Cabuk, S.; Simsek, S. First-principles calculation of the linear and nonlinear optical properties of $LiTaO_3$. *Phys. Scr.* **2010**, *81*, 223–232. [CrossRef]
95. Cho, Y.; Hashimoto, S.; Odagawa, N.; Tanaka, K.; Hiranaga, Y. Nanodomain manipulation for ultrahigh density ferroelectric data storage. *Nanotechnology* **2006**, *17*, 137–141. [CrossRef]
96. Takahashi, H.; Mimura, Y.; Mori, S.; Ishimori, M.; Onoe, A.; Ono, T.; Esashi, M. The fabrication of metallic tips with a silicon cantilever for probe-based ferroelectric data storage and their durability experiments. *Nanotechnology* **2009**, *20*, 365201. [CrossRef] [PubMed]
97. Chu, W.-S.; Kim, S.-M.; Wu, X.; Wen, L.; Oh, M.-C. Optical voltage sensors based on integrated optical polarization-rotated reflection interferometry. *J. Light. Technol.* **2016**, *34*, 2170–2174. [CrossRef]
98. Cheng, C.; Jia, Y.; de Aldana, J.R.V.; Tan, Y.; Chen, F. Hybrid waveguiding structure in $LiTaO_3$ crystal fabricated by direct femtosecond laser writing. *Opt. Mater.* **2016**, *51*, 190–193. [CrossRef]
99. Katz, M.; Route, R.K.; Hum, D.S.; Parameswaran, K.R.; Miller, G.D.; Fejer, M.M. Vapor-transport equilibrated near-stoichiometric lithium tantalate for frequency-conversion applications. *Opt. Lett.* **2004**, *29*, 1775–1777. [CrossRef] [PubMed]
100. Brinkmann, R.; Sohler, W. Continuous-wave erbium-diffused $LiNbO_3$ waveguide laser. *Electron. Lett.* **1991**, *27*, 415–417. [CrossRef]
101. Fan, T.Y.; Cordova-Plaza, A.; Digonnet, M.J.F.; Byer, R.L.; Shaw, H.J.J. Nd:MgO:$LiNbO_3$ spectroscopy and laser devices. *J. Opt. Soc. Am. B* **1986**, *3*, 140–148. [CrossRef]
102. Li, Y.; Li, J.; Zhou, Z.; Guo, R.; Bhalla, A.S. Low-frequency–dependent electro-optic properties of potassium lithium tantalate niobate single crystals. *Europhys. Lett.* **2013**, *102*, 37004–37007. [CrossRef]
103. Wu, C.C.; Hsu, W.T.; Chen, Z.B.; Choubey, R.K.; Lan, C.W. Crystal growth, VTE treatment, and characterizations of Nd-doped $LiTaO_3$. *J. Cryst. Growth* **2011**, *318*, 649–652. [CrossRef]
104. Hsu, W.T.; Chen, Z.B.; Wu, C.C.; Choubey, R.K.; Lan, C.W. Optical Properties of Mg, Fe, Co-Doped Near-Stoichiometric $LiTaO_3$ Single Crystals. *Materials* **2012**, *5*, 227–238. [CrossRef]
105. Dolev, I.; Ganany-Padowicz, A.; Gayer, O.; Arie, A.; Mangin, J.; Gadret, G. Linear and nonlinear optical properties of MgO:$LiTaO_3$. *Appl. Phys. B Lasers Opt.* **2009**, *96*, 423–432. [CrossRef]
106. Sokólska, I.; Ryba-Romanowski, W.; Gołab, S.; Lukasiewicz, T. The optical properties of Yb^{3+} ions in $LiTaO_3$:Nd,Yb crystals. *Appl. Phys. B* **1997**, *65*, 495–498.
107. Nakamura, K.; Kurz, J.; Parameswaran, K.; Fejer, M.M. Periodic poling of magnesium-oxide-doped lithium niobate. *Am. Inst. Phys.* **2002**, *91*, 4528–4534. [CrossRef]
108. Saikawa, J.; Fujii, M.; Ishizuki, H.; Taira, T. 52 mJ narrow-bandwidth degenerated optical parametric system with a large-aperture periodically poled MgO:$LiNbO_3$ device. *Opt. Lett.* **2006**, *31*, 3149–3151. [CrossRef]
109. Kar, S.; Choubey, R.K.; Sen, P.; Bhagavannarayana, G.; Bartwal, K.S. Studies on codoping behavior of Nd:Mg:$LiNbO_3$ crystals. *Phys. B Condens. Matter* **2007**, *393*, 37–42. [CrossRef]
110. Pang, C.; Li, R.; Li, Z.; Dong, N.; Wang, J.; Ren, F.; Chen, F. Plasmonic Ag nanoparticles embedded in lithium tantalate crystal for ultrafast laser generation. *Nanotechnology* **2019**, *30*, 334001. [CrossRef]
111. Shur, V.Y. Domain nanotechnology in ferroelectric single crystals: Lithium niobate and lithium tantalate family. *Ferroelectrics* **2013**, *443*, 71–82. [CrossRef]
112. Feng, T.; Li, T.; Zhao, S.; Li, Q.; Yang, K.; Zhao, J.; Qiao, W.; Hang, Y.; Zhang, P.; Wang, Y. Performance of diode-pumped continuous wave tunable and passively Q-switched Nd,Mg:$LiTaO_3$ laser. *Opt. Commun.* **2014**, *325*, 92–94. [CrossRef]
113. Denton, R.T.; Chen, F.S.; Ballman, A.A. Lithium Tantalate Light Modulators. *J. Appl. Phys.* **1967**, *38*, 1611–1617. [CrossRef]
114. Cui, S.; Qian, J.; Zeng, X.; Cheng, X.; Gu, X.; Feng, Y. A watt-level yellow random laser via single-pass frequency doubling of a random Raman fiber laser. *Opt. Fiber Technol.* **2021**, *64*, 102552. [CrossRef]
115. Meyn, J.-P.; Fejer, M. Tunable ultraviolet radiation by second-harmonic generation in periodically poled lithium tantalate. *Opt. Lett.* **1997**, *22*, 1214–1216. [CrossRef]
116. Song, P. *Research on Channel Transmission Characteristics of Wireless Ultraviolet Mobile Ad Hoc Networks*; Xi'an University Of Technology: Xi'an, China, 2017.

117. Meyn, J.P.; Laue, C.; Knappe, R.; Wallenstein, R.; Fejer, M.M. Fabrication of periodically poled lithium tantalate for UV generation with diode lasers. *Appl. Phys. B* **2001**, *73*, 111–114. [CrossRef]
118. Rimeika, R.; Čiplys, D.; Jonkus, V.; Shur, M. Acoustoelectric effects in reflection of leaky-wave-radiated bulk acoustic waves from piezoelectric crystal-conductive liquid interface. *Ultrasonics* **2016**, *64*, 196–199. [CrossRef]
119. Li, L.Q.; Zhang, B.; Romero, C.; Aldana, J.; Chen, F. Tunable violet radiation in a quasi-phase-matched periodically poled stoichiometric lithium tantalate waveguide by direct femtosecond laser writing. *Results Phys.* **2020**, *19*, 103373. [CrossRef]
120. Wu, B.; Zhang, B.; Liu, W.; Lu, Q.; Wang, L.; Chen, F. Recoverable and rewritable waveguide beam splitters fabricated by tailored femtosecond laser writing of lithium tantalate crystal. *Opt. Laser Technol.* **2022**, *145*, 107500. [CrossRef]
121. Dong, H.R.; Cao, Q.T.; Zhang, P.; Lu, B. Terahertz pyroelectric detector based on lithium tantalate wafer. *J. Infrared* **2020**, *41*, 14–19.
122. Zhang, D.Y. *Principle and Preparation of Pyroelectric Lithium Tantalate Thin Film Infrared Detector*; University of Electronic Science and Technology of China: Chengdu, China, 2008.
123. Arose, C.; Terracciano, A.C.; Peale, R.E.; Gonzalez, F.J.; Loparo, Z.; Cetnar, J.; Vasu, S.S. Far-infrared spectrally selective $LiTaO_3$ and AlN pyroelectric detectors using resonant subwavelength metal surface structures. *MRS Adv.* **2020**, *5*, 2005–2012. [CrossRef]
124. Peng, S.C.; Zhang, R.X.; Yang, H.; Qiu, Z.L.; Li, Y.F.; Wen, Z.R.; Tang, P.; Dong, S. Crystal filter with high fundamental frequency and high electromechanical coupling coefficient. *J. Piezoelectrics Acoustooptics* **2020**, *42*, 761–764.
125. Qi, M.K. Research on High Temperature Strain Sensor Based on Surface Acoustic Wave (SAW) Technology. Ph.D. Dissertation, Chongqing University, Chongqing, China, 2019.
126. Kim, C.U.; Balashov, S.M.; Plessky, V.P.; Nam, C.W.; Lee, K.C. Ladder-type SAW filters using thinned density of randomly distributed "hot" electrodes. *IEEE Trans. Ultrason. Ferroelectr. Freq. Control.* **2010**, *57*, 2585–2587. [CrossRef]
127. Cheng, X.Y.; Zhou, Z.; Peng, S.C. Miniaturized bandwidth lithium tantalate crystal filter. *J. Piezoelectrics Acoustooptics* **2011**, *33*, 386–389.
128. Peng, S.C.; Chen, X.Y.; Liu, G.C. Development of high-frequency broadband lithium tantalate crystal filter. *J. Piezoelectrics Acoustooptics* **2009**, *28*, 141–143.
129. Tanaka, S.; Kadota, M. IDT-based acoustic wave devices using ultrathin lithium niobate and lithium tantalate. In Proceedings of the 2020 Joint Conference of the IEEE International Frequency Control Symposium and International Symposium on Applications of Ferroelectrics (IFCS-ISAF), Keystone, CO, USA, 19–23 July 2020; pp. 1–3.
130. Ballandras, S.; Courjon, E.; Baron, T.; Moulet, J.B.; Signamarcheix, T.; Daniau, W. $LiTaO_3$/silicon composite wafers for the fabrication of low loss low TCF high coupling resonators for filter applications. In Proceedings of the International Symposium on Applications of Ferroelectric, Singapore, 24–27 May 2015.
131. Assila, N.; Kadota, M.; Tanaka, S. High-frequency resonator using A 1 Lamb wave mode in $LiTaO_3$ plate. *IEEE Trans. Ultrason. Ferroelectr. Freq. Control.* **2019**, *66*, 1529–1535. [CrossRef]
132. Naumenko, N.F. High-velocity non-attenuated acoustic waves in $LiTaO_3$/quartz layered substrates for high frequency resonators. *Ultrasonics* **2019**, *95*, 1–5. [CrossRef]
133. Nishi, H.; Tsuchizawa, T.; Segawa, T.; Matsuo, S. Low-loss lithium tantalate on insulator waveguide towards on-chip nonlinear photonics. In Proceedings of the 2022 27th OptoElectronics and Communications Conference (OECC) and 2022 International Conference on Photonics in Switching and Computing (PSC), Toyama, Japan, 3–6 July 2022; pp. 1–3.